Theoretical modeling of resonant laser excitation of atoms in a magnetic field

Andrew James Murray,[1] William MacGillivray,[1,2] and Martyn Hussey[1]

[1]*School of Physics and Astronomy, University of Manchester, Manchester M13 9PL, United Kingdom*
[2]*Southern Cross University, Lismore NSW 2480, Australia*
(Received 25 September 2007; published 23 January 2008)

The interaction of near-resonant laser radiation with atoms immersed in a magnetic **B** field is calculated using a quantum electrodynamic model. In this model, the magnetic field is assumed to produce a small perturbation such that the degeneracy of the magnetic substates is lifted while maintaining the usual quantum numbers that define the states (the Zeeman effect). The laser radiation is considered to have a narrow bandwidth and to be temporally and spatially coherent. The model produces three general coupled differential equations that describe the state populations and their relative coherences and the optical coherences between levels coupled by the laser radiation. The model can therefore be directly applied to different experiments ranging from atom trapping and cooling experiments through to collision experiments carried out in magnetic and laser fields.

PACS number(s): 32.60.+i, 32.80.Xx, 34.80.Dp, 34.80.Qb

I. INTRODUCTION

The application of laser radiation to atomic or molecular targets immersed in magnetic fields is now widely used in many different experiments. Such experiments include the production of slow atoms from effusive sources in a Zeeman slower and the cooling and trapping of atoms to microkelvin temperatures in a magneto-optical trap (MOT) [1]. New collision experiments have also been performed where atoms are prepared in an excited state within a magnetic field produced by a magnetic angle changing (MAC) device [2], so that the differential cross section can be obtained for electron collisions over all scattering geometries [3,4]. In such experiments, the magnetic field steers electrons to and from the interaction region where the laser-excited targets are located.

In each of these examples, the targets are immersed in both a magnetic **B** field and a near-resonant laser field. To accurately reveal the dynamics of these interactions, it is necessary to adopt a model that allows the equations of motion of the system to be derived. In most cases studied so far, the system is assumed to occupy only two states so that simple rate equations can be formulated [1]. This approach is used extensively in trapping and cooling experiments to predict the reaction of the atoms to the field. However, these experiments are then restricted to those involving circularly polarized radiation where the system is closed (i.e., only two states are coupled by the laser radiation). Although this is a valuable and simple model, it is more appropriate to use a theory that involves *all* participating states of the system, that allows for different polarization states of the laser and that is tractable to the experimentalist.

New experiments have now been performed in which the simple two-state model cannot be applied. In these experiments, an atom is prepared in an excited state using laser radiation prior to electron impact excitation [5], deexcitation [4], or ionization [6] of the target. In each case, it can be advantageous to employ a MAC device so that the electrons that participate in the collision are steered into and out of the interaction region over all scattering geometries from 0° to 180° [2,6,7]. The MAC device has recently been employed

in superelastic scattering experiments from laser-excited calcium atoms [4], and so it is essential to develop a model of the laser interaction to fully describe the collision process under study. An example of how this model is applied to superelastic scattering of electrons from calcium is given in Sec. IV below.

The criteria chosen in the development of the model are as follows. The magnetic **B** field is assumed to be relatively weak so that the total angular momentum of the target remains a good quantum number (the Zeeman effect). In this case, the laser interaction requires an atom to be described in either J representation (for targets that do not possess nuclear spin, such as ^{40}Ca) or in F representation (for targets with a nonzero nuclear spin, such as the alkali-metal atoms). The second criterion is that the laser radiation is assumed to be sufficiently weak that multiphoton processes can be neglected. The dipole approximation is therefore used, and the harmonic approximation (which assumes the operator elements evolve freely during the laser interaction) is adopted. The state of the system is derived from expectation values of the operators with the assumption that the dynamics varies slowly compared to the oscillation frequency of the laser field. The model is therefore not applicable for radiation in the fs temporal regime. Finally, normal ordering is chosen in the usual way when describing the laser field interaction with the targets [8].

These criteria restrict the model to laser intensities typically less than $\sim 10^{12}$ W/cm^2 and to lasers with coherence times of picoseconds or longer. As such, the model can be applied to all cases involving high-resolution cw lasers (such as the cooling, trapping, and collision experiments described above) and to pulsed laser experiments that satisfy these criteria.

This paper is divided into five sections. Following this Introduction, the theory is described and the general equations of motion derived. Specific coupled rate equations are then formulated for a $J=0$ to $J=1$ transition (as in calcium excitation from the ground state) so as to illustrate the model. The example systems are divided into two cases: that of circularly polarized laser excitation directed along the **B**-field

direction and that of linearly polarized laser excitation where the applied **B** field is orthogonal to the polarization vector of the laser. Examples of the dynamics of the interaction are also presented.

The steady-state solutions are then derived for the $J=0$ to $J=1$ transition, and it is shown that these are considerably more complex than for the two-state system when linearly polarized radiation is used. From these equations, the effects of the combined magnetic and electric fields are derived in terms of a density matrix describing the "shape" and orientation of the excited P-state atom in an analogous way to that used to describe atoms excited by electron impact. Finally, the application of the model to the superelastic scattering process in a MAC device is presented.

II. QED THEORY FOR THE INTERACTION OF LASER AND MAGNETIC FIELDS WITH A TARGET

In the following description of the QED theory, we follow the work of Farrell, MacGillivray, and Standage [9], who derived the equations of motion for superelastic scattering studies from sodium. The Hamiltonian used in this previous work is modified here to include the effects of the magnetic field, which is treated as a perturbation. The description is in the Heisenberg picture in which the operators are time dependent. By moving to the reference frame of the laser field, the operators are transformed to slowly varying terms whose expectation values directly relate to density matrix elements describing the populations and coherences between states coupled by the radiation field.

Consider first the Hamiltonian, which describes the interaction of an atomic target with a laser field and a weak magnetic field. This may be written

$$H = H_{atom} + H_{field} + H_{interaction}$$
$$= [H_{free} + H_{B\ field}] + H_{field} + H_{interaction}, \quad (1)$$

where

$$H_{atom} = H_{free} + H_{B\ field} = \underbrace{\sum_i \hbar\omega_i |i\rangle\langle i|}_{H_{free}} + \underbrace{\frac{\mu_B g_{J(F)}}{\hbar}\mathbf{J}(\mathbf{F})\cdot\mathbf{B}}_{H_{B\ field}}$$

$$= \sum_i \hbar\omega_i |i\rangle\langle i| + \left(\frac{\mu_B g_{J(F)}|\mathbf{B}|}{\hbar}\right)\mathbf{J}(\mathbf{F})\cdot\hat{\mathbf{B}}, \quad (2)$$

$\omega_{BJ(F)} = \frac{\mu_B g_{J(F)}|\mathbf{B}|}{\hbar}$ is the Larmor precession frequency, μ_B is the Bohr magneton, and $g_{J(F)}$ is the Lande g factor either in J or F representation [10]. Equation (2) can be written in either representation, so J will be used from this point for simplicity.

The Hamiltonian for the coherent laser field may be written in terms of annihilation and creation operators in the usual way:

$$H_{field} = \sum_{\lambda'} \hbar\omega_{\lambda'} a^\dagger_{\lambda'} a_{\lambda'}, \quad (3)$$

where the mode index λ' specifies the polarization $\hat{\varepsilon}_{\lambda'}$ and wave vector $\mathbf{k}_{\lambda'}$ of the laser field. The interaction Hamil-

tonian that physically describes the coupling of the laser field to the atom is given by [8]

$$H_{interaction} = \sum_{\lambda',e',g'} \hbar(g^{\lambda'}_{e'g'}\hat{\sigma}_{e'g'}a_{\lambda'}e^{+ik_{\lambda'}z}$$
$$+ g^{\lambda'*}_{e'g'}a^\dagger_{\lambda'}e^{-ik_{\lambda'}z}\hat{\sigma}_{g'e'}), \quad (4)$$

where $g^{\lambda'}_{e'g'} = i\sqrt{\frac{\omega_{\lambda'}}{2\varepsilon_0\hbar V}}\hat{\varepsilon}_{\lambda'}\cdot\mathbf{D}_{e'g'}$ is a coupling coefficient between the laser field mode and atomic states $|g'\rangle, |e'\rangle$, with V being the mode volume and $\mathbf{D}_{e'g'}$ the dipole moment. The atomic operators are given by the outer product of state vectors that define the atomic system:

$$\hat{\sigma}_{ij} = |i\rangle\langle j|. \quad (5)$$

Since the field and atomic operators commute, the ordering of Eq. (4) is arbitrary. However, by writing Eq. (4) in *normal ordering* as above, it is then possible to directly relate the results of further operations to the classical analogies of spontaneous emission due to radiation reaction of the source Coulomb field upon itself [11].

The derivation of the Heisenberg operator equations of motion is calculated in the usual way. For operators $\hat{\sigma}_{eg}$ between the lower states $|g\rangle$ and upper excited states $|e\rangle$, this is given by

$$\frac{d\hat{\sigma}_{eg}}{dt} = -\frac{i}{\hbar}[\hat{\sigma}_{eg},H] = \underbrace{-\frac{i}{\hbar}[\hat{\sigma}_{eg},H_{atom}]}_{term\ 1} \underbrace{-\frac{i}{\hbar}[\hat{\sigma}_{eg},H_{int}]}_{term\ 2}.$$
$$(6)$$

H_{field} does not contribute since it commutes with the atomic operator. By appropriate manipulation of the above equations, term 1 is given by

$$\underbrace{-\frac{i}{\hbar}[\hat{\sigma}_{eg},H_{atom}]}_{term\ 1} = -i\left\{(\omega_g - \omega_e)|e\rangle\langle g| + \left[|e\rangle\langle g|\left(\frac{\mu_B g_J B}{\hbar^2}\right)\mathbf{J}\cdot\hat{\mathbf{B}}\right.\right.$$
$$\left.\left. - \left(\frac{\mu_B g_J B}{\hbar^2}\right)\mathbf{J}\cdot\hat{\mathbf{B}}|e\rangle\langle g|\right]\right\}. \quad (7)$$

The derivation of term 2 is considerably more involved. Since the field mode couples to the atom, the time dependence of $a^\dagger_{\lambda'}$, and $a_{\lambda'}$ depends on the atomic-state ensemble and the coupling coefficients. By appropriate manipulation of the operator equation, it can be shown that

$$a_{\lambda'}(t) = a_{\lambda'}(0)e^{-i\omega_{\lambda'}t}$$
$$- i\sum_{e'',g''} g^{\lambda'*}_{e''g''}e^{-ik_{\lambda'}z}\int_0^t \hat{\sigma}_{g''e''}(t')e^{-i\omega_{\lambda'}(t-t')}dt',$$

$$a^\dagger_{\lambda'}(t) = a^\dagger_{\lambda'}(0)e^{+i\omega_{\lambda'}t}$$
$$+ i\sum_{e'',g''} g^{\lambda'}_{e''g''}e^{ik_{\lambda'}z}\int_0^t \hat{\sigma}_{e''g''}(t')e^{+i\omega_{\lambda'}(t-t')}dt'. \quad (8)$$

Substituting Eqs. (8) into term 2 and by invoking the Harmonic approximation, it can be shown that

$$-\frac{i}{\hbar}[\hat{\sigma}_{eg}, H_{int}] = -i \sum_{\lambda',e'} g_{e'g}^{\lambda'*} a_{\lambda'}^{\dagger}(0) e^{+i(\omega_{\lambda'}t - k_{\lambda'}z)} \hat{\sigma}_{ee'}$$

$$+ i \sum_{\lambda',g'} g_{eg'}^{\lambda'*} a_{\lambda'}^{\dagger}(0) e^{+i(\omega_{\lambda'}t - k_{\lambda'}z)} \hat{\sigma}_{g'g}$$

$$+ \sum_{\lambda',e'} \left(\sum_{e'',g''} g_{e'g}^{\lambda'*} g_{e''g''}^{\lambda'} \hat{\sigma}_{e''g''} \right.$$

$$\left. \times \int_0^t e^{+i(\omega_{\lambda'} - \omega_{e''} + \omega_{g''})(t-t')} dt' \right) \hat{\sigma}_{ee'}$$

$$- \sum_{\lambda',g'} \left(\sum_{e'',g''} g_{eg'}^{\lambda'*} g_{e''g''}^{\lambda'} \hat{\sigma}_{e''g''} \right.$$

$$\left. \times \int_0^t e^{+i(\omega_{\lambda'} - \omega_{e''} + \omega_{g''})(t-t')} dt' \right) \hat{\sigma}_{g'g}. \quad (9)$$

The integrals in Eq. (9) are evaluated in the usual way for interaction times large compared to the characteristic time associated with detuning and can be approximated to δ functions [8,11]. The complete operator equation is thus given by summing terms 1 and 2:

$$\frac{d\hat{\sigma}_{eg}}{dt} = -i\left((\omega_g - \omega_e)\hat{\sigma}_{eg} + \frac{\mu_B B}{\hbar^2}(\hat{\sigma}_{eg} g_J \mathbf{J} \cdot \hat{\mathbf{B}} - g_J \mathbf{J} \cdot \hat{\mathbf{B}} \hat{\sigma}_{eg}) \right)$$

$$- i \sum_{\lambda',e'} g_{e'g}^{\lambda'*} a_{\lambda'}^{\dagger}(0) e^{+i(\omega_{\lambda'}t - k_{\lambda'}z)} \hat{\sigma}_{ee'}$$

$$+ i \sum_{\lambda',g'} g_{eg'}^{\lambda'*} a_{\lambda'}^{\dagger}(0) e^{+i(\omega_{\lambda'}t - k_{\lambda'}z)} \hat{\sigma}_{g'g}$$

$$- \sum_{\lambda',g',e'} g_{eg'}^{\lambda'*} g_{e'g}^{\lambda'} \hat{\sigma}_{e'g} \pi \delta(\omega_{\lambda'} - \omega_{e'} + \omega_{g'}). \quad (10)$$

To establish expectation values, the atomic operators $\hat{\sigma}_{ij}$ are transformed to slowly varying operators χ_{ij}:

$$\hat{\sigma}_{eg} = \chi_{eg} e^{i(\omega_L t - k_L z)}, \quad \hat{\sigma}_{gg'} = \chi_{gg'}; \hat{\sigma}_{ee'} = \chi_{ee'}, \quad (11)$$

and so

$$\frac{d\hat{\sigma}_{eg}}{dt} = \frac{d\chi_{eg}}{dt} e^{i(\omega_L t - k_L z)} + i\omega_L \chi_{eg} e^{i(\omega_L t - k_L z)} - ik_L \frac{dz}{dt} \chi_{eg} e^{i(\omega_L t - k_L z)}$$

$$= \dot{\chi}_{eg} e^{i(\omega_L t - k_L z)} + i(\omega_L - k_L v_z) \chi_{eg} e^{i(\omega_L t - k_L z)}. \quad (12)$$

Taking expectation values, the equation of motion then becomes

$$\langle \dot{\chi}_{eg} \rangle = -i\left((\omega_L - k_L v_z - \omega_{eg})\langle \chi_{eg} \rangle \right.$$

$$+ \frac{\mu_B B}{\hbar^2} \langle \chi_{eg} g_J \mathbf{J} \cdot \hat{\mathbf{B}} - g_J \mathbf{J} \cdot \hat{\mathbf{B}} \chi_{eg} \rangle \bigg)$$

$$- i \sum_{\lambda',e'} g_{e'g}^{\lambda'*} \langle a_{\lambda'}^{\dagger}(0) \rangle \langle \chi_{ee'} \rangle e^{+i[(\omega_{\lambda'} - \omega_L)t - (k_{\lambda'} - k_L)z]}$$

$$+ i \sum_{\lambda',g'} g_{eg'}^{\lambda'*} \langle a_{\lambda'}^{\dagger}(0) \rangle \langle \chi_{g'g} \rangle e^{+i[(\omega_{\lambda'} - \omega_L)t - (k_{\lambda'} - k_L)z]}$$

$$- \sum_{\lambda',g',e'} g_{eg'}^{\lambda'*} g_{e'g}^{\lambda'} \langle \chi_{e'g} \rangle \pi \delta(\omega_{\lambda'} - \omega_{e'} + \omega_{g'}). \quad (13)$$

Assuming coherent laser excitation (e.g., from a high-resolution laser operating far above threshold) and noting that the laser field can be written in terms of coherent states [8], we set $\lambda' = L$ in the driving terms so that

$$\langle \dot{\chi}_{eg} \rangle = -i\left(\Delta_{L,eg} \langle \chi_{eg} \rangle + \frac{\mu_B B}{\hbar^2} \langle \chi_{eg} g_J \mathbf{J} \cdot \hat{\mathbf{B}} - g_J \mathbf{J} \cdot \hat{\mathbf{B}} \chi_{eg} \rangle \right)$$

$$- i \sum_{L,e'} \Omega_{e'g}^{L} \langle \chi_{ee'} \rangle + i \sum_{L,g'} \Omega_{eg'}^{L} \langle \chi_{g'g} \rangle$$

$$- \sum_{\lambda,g',e'} g_{eg'}^{\lambda*} g_{e'g}^{\lambda} \langle \chi_{e'g} \rangle \pi \delta(\omega_{\lambda} - \omega_{e'} + \omega_{g'}), \quad (14)$$

where the Doppler detuning is given by

$$\Delta_{L,eg} = \omega_L - k_L v_z - (\omega_e - \omega_g) = \omega_L - k_L v_z - \omega_{eg} \quad (15)$$

and the on-resonance half Rabi frequency (set to be real by an appropriate choice of phase) is given by

$$\Omega_{eg}^{L} = g_{eg}^{L*} \langle a_L^{\dagger}(0) \rangle = g_{eg}^{L} \langle a_L(0) \rangle, \quad (16)$$

where expectation values are taken over the coherent states of the laser field. The Rabi frequency can be directly calculated from the intensity of the laser radiation and lifetime of the upper excited state (see, for example, [12,13]).

In a similar way as shown above, the equations of motion for substates in the same level can be derived. For the upper laser-excited state,

$$\langle \dot{\chi}_{e''e} \rangle = -i\left((\omega_e - \omega_{e''})\langle \chi_{e''e} \rangle + \frac{\mu_B B}{\hbar^2} \langle \chi_{e''e} g_J \mathbf{J} \cdot \hat{\mathbf{B}} \right.$$

$$\left. - g_J \mathbf{J} \cdot \hat{\mathbf{B}} \chi_{e''e} \right) - i \sum_{L,g'} \Omega_{eg'}^{L} \langle \chi_{e''g'} \rangle$$

$$- \sum_{\lambda',g',e'} g_{eg'}^{\lambda'} g_{e'g'}^{\lambda'*} \pi \delta(\omega_{e'} - \omega_{g'} - \omega_{\lambda'}) \langle \chi_{e''e'} \rangle$$

$$+ i \sum_{L,g'} \Omega_{e''g'}^{L} \langle \chi_{g'e} \rangle - \sum_{\lambda',g',e'} g_{e''g'}^{\lambda'*} g_{e'g'}^{\lambda'}$$

$$\times \pi \delta(\omega_{\lambda'} - \omega_{e'} + \omega_{g'}) \langle \chi_{e'e} \rangle, \quad (17)$$

whereas for the lower state,

$$\langle \dot{\chi}_{g''g} \rangle = -i \Bigg((\omega_g - \omega_{g''}) \langle \chi_{g''g} \rangle + \frac{\mu_B B}{\hbar^2} \langle \chi_{g''g} g_J \mathbf{J} \cdot \hat{\mathbf{B}}$$

$$- g_J \mathbf{J} \cdot \hat{\mathbf{B}} \chi_{g''g} \Bigg) + i \sum_{L,e'} \Omega^L_{e'g''} \langle \chi_{e'g} \rangle$$

$$+ \sum_{\lambda',e',e'''} g^{\lambda'}_{e'g} g^{\lambda'*}_{e'''g} \langle \chi_{e'e'''} \rangle$$

$$\times \pi \delta(\omega_{e'''} - \omega_g - \omega_{\lambda'}) - i \sum_{L,e'} \Omega^L_{e'g} \langle \chi_{g''e'} \rangle$$

$$+ \sum_{\lambda',e',e'''} g^{\lambda'*}_{e'g} g^{\lambda'}_{e'''g''} \langle \chi_{e'''e'} \rangle \pi \delta(\omega_{\lambda'} + \omega_{g''} - \omega_{e'''}). \tag{18}$$

A. Choice of quantization axis

Equations (14)–(18) are general equations that define the dynamics of the system under the influence of a laser field and a magnetic field. To proceed further, a quantization axis is defined so that measurements can be taken. In the case presented here, the quantization axis (z axis) is chosen parallel to the magnetic field $\hat{\mathbf{B}}$. The expectation values of the magnetic terms can then be derived.

As an example, consider the magnetic terms in Eq. (14):

$$\left(\frac{\mu_B B}{\hbar^2} \right) \langle \chi_{eg} g_J \mathbf{J} \cdot \hat{\mathbf{B}} - g_J \mathbf{J} \cdot \hat{\mathbf{B}} \chi_{eg} \rangle$$

$$= \left(\frac{\mu_B B}{\hbar^2} \right) (\langle \psi | e \rangle \langle g | g_J \mathbf{J} \cdot \hat{\mathbf{B}} | \psi \rangle - \langle \psi | g_J \mathbf{J} \cdot \hat{\mathbf{B}} | e \rangle \langle g | \psi \rangle). \tag{19}$$

Since $\mathbf{z} \| \hat{\mathbf{B}}$, we have

$$\left(\frac{\mu_B B}{\hbar^2} \right) (\langle \psi | e \rangle \langle g | g_J \mathbf{J} \cdot \hat{\mathbf{B}} | \psi \rangle - \langle \psi | g_J \mathbf{J} \cdot \hat{\mathbf{B}} | e \rangle \langle g | \psi \rangle)$$

$$= \left(\frac{\mu_B B}{\hbar^2} \right) (\langle \psi | e \rangle \langle g | g_J J_z | \psi \rangle - \langle \psi | g_J J_z | e \rangle \langle g | \psi \rangle)$$

$$= (\omega_{BJ_g} m_g - \omega_{BJ_e} m_e) \langle \chi_{eg} \rangle. \tag{20}$$

The expectation values of the slowly varying operators are directly related to the density matrix elements more commonly used to define the atomic states:

$$\langle \chi_{eg} \rangle = \langle \psi | e \rangle \langle g | \psi \rangle = (\langle e | \psi \rangle \langle \psi | g \rangle)^* = \rho^*_{eg} = \rho_{ge}. \tag{21}$$

The equations of motion (choosing the z axis along the **B**-field direction) are then given for lower-state populations ($g = g''$) and atomic coherences ($g \neq g''$) by:

$$\dot{\rho}_{gg''} = -i(\omega_g - \omega_{g''} + \omega_{BJ_g} m_g - \omega_{BJ_{g''}} m_{g''}) \rho_{gg''} + i \sum_{L,e} \Omega^L_{eg''} \rho_{ge}$$

$$- i \sum_{L,e} \Omega^L_{eg} \rho_{eg''} + \sum_{\lambda,e',e''} g^\lambda_{e'g''} g^{\lambda*}_{e''g} \pi \delta(\Delta_{e''g} - \omega_\lambda) \rho_{e''e'}$$

$$+ \sum_{\lambda,e',e''} g^{\lambda*}_{e'g} g^\lambda_{e''g''} \pi \delta(\Delta_{e''g} - \omega_\lambda) \rho_{e'e''}; \tag{22}$$

Upper state populations ($e = e''$) and atomic coherences ($e \neq e''$) by:

$$\dot{\rho}_{ee''} = -i(\omega_e - \omega_{e''} + \omega_{BJ_e} m_e - \omega_{BJ_{e''}} m_{e''}) \rho_{ee''} + i \sum_{L,g} \Omega^L_{e''g} \rho_{eg}$$

$$- i \sum_{L,g} \Omega^L_{eg} \rho_{ge''} - \sum_{\lambda,g',e'} g^\lambda_{eg'} g^{\lambda*}_{e'g'} \pi \delta(\Delta_{e'g'} - \omega_\lambda) \rho_{e'e''}$$

$$- \sum_{\lambda,g',e'} g^{\lambda*}_{e''g'} g^\lambda_{e'g'} \pi \delta(\Delta_{e'g'} - \omega_\lambda) \rho_{ee'}, \tag{23}$$

and optical ($e = g \pm 1, 0$) and non-optical ($e \neq g \pm 1, 0$) coherences between lower and upper states by:

$$\dot{\rho}_{ge} = -i(\Delta_{L,eg} + \omega_{BJ_g} m_g - \omega_{BJ_e} m_e) \rho_{ge} - i \sum_{L,e'} \Omega^L_{e'g} \rho_{e'e}$$

$$+ i \sum_{L,g'} \Omega^L_{eg'} \rho_{gg'} - \sum_{\lambda,g',e'} \rho_{ge'} g^{\lambda*}_{eg'} g^\lambda_{e'g'} \pi \delta(\Delta_{e'g'} - \omega_\lambda), \tag{24}$$

where $\Delta_{eg} = \omega_e - \omega_g$ and other terms are as stated. These equations can be summarized into a single matrix equation

$$\dot{\underset{\sim}{\rho}} = \underset{\approx}{A} \underset{\sim}{\rho}, \tag{25}$$

where ρ is a column vector with elements ρ_{ij} and A is a complex matrix defined by Eqs. (22)–(24).

The coupled differential equations (22)–(24) are a general set of equations that can be applied to any system with the proviso that the quantization axis is along the direction of the magnetic **B** field. The first terms are oscillatory terms between substates of the same state ensemble and may lead to quantum beats or **B**-field-induced oscillations. Terms involving the Rabi frequency are coherent driving terms that result in absorption of photons from the laser field and stimulated emission of photons into the laser field. The Rabi frequency is directly proportional to the magnitude of the electric field [8], and so the probability of absorption and stimulated emission processes is proportional to the square root of the laser intensity.

The triple sums in Eqs. (22)–(24) arise from spontaneous emission of photons. These relaxation terms arise even when there are no driving terms (i.e., when $\Omega^L_{eg} = 0$) and lead to damping of any oscillations over time. They can be represented by a set of generalized decay constants where

$$\Gamma_{ege'g'} = \sum_{\lambda'} [g^{\lambda'}_{e'g'} g^{\lambda'*}_{eg} \pi \delta(\Delta_{e'g'} - \omega_{\lambda'})$$

$$+ g^{\lambda'}_{e'g'} g^{\lambda'*}_{eg} \pi \delta(\Delta_{eg} - \omega_{\lambda'})]$$

$$\Rightarrow \Gamma_{eg} = \Gamma_{egeg} = 2 \sum_{\lambda'} |g^{\lambda'}_{eg}|^2 \pi \delta(\Delta_{eg} - \omega_{\lambda'})$$

$$\Rightarrow \Gamma_e = \sum_g \Gamma_{eg} = 2 \sum_g \sum_{\lambda'} |g^{\lambda'}_{eg}|^2 \pi \delta(\Delta_{eg} - \omega_{\lambda'}). \tag{26}$$

Note that should state $|g\rangle$ *not* be the lowest state, an additional term must be included in Eq. (22) to allow for spontaneous decay from $|g\rangle$ to all lower states that are optically
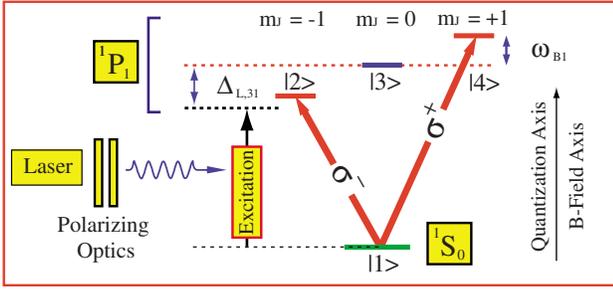
FIG. 1. (Color online) Application of a weak **B** field removes the degeneracy of the states as shown. The laser is tuned near resonant to the atomic transition, such that the detuning from resonance is $\Delta_{L,31}$. The figure shows excitation by σ^+ and σ^- radiation, where the quantization axes for the laser (along the beam direction) and the **B** field are the same.

accessible. Additionally, if the upper state $|e\rangle$ can relax to states other than state $|g\rangle$, additional spontaneous emission terms must be included to allow for these transitions. These extra decay terms are fully described in [12,13].

III. EXAMPLE: DERIVATION OF THE EQUATIONS OF MOTION FOR *S* TO *P* TRANSITIONS

As an example of the use of Eqs. (22)–(24) in an experiment, consider laser transitions from an *S* state to a *P* state under the action of a weak **B** field, as shown in Fig. 1. In this case, the laser is near resonance (detuning $\Delta_{L,31}$ from the $|J,m_J\rangle = |1,0\rangle$ state) and the Larmor frequency is ω_{B1} for the upper state. Since the ground state is singlet, $\omega_{B0} = 0$. The coupling coefficients $g_{eg}^{\lambda'}$ that are nonzero are then given by g_{21}^{-1}, g_{31}^{0}, and g_{41}^{+1}.

Two cases are presented to illustrate how the equations of motion are calculated. In the first, the laser radiation is circularly polarized and is directed along the **B**-field axis. The preferred quantization axis of the **B** field and the laser are then the same, so that transitions occur with $\Delta m_J = \pm 1$ for $\sigma^{\pm}$ radiation, as in Fig. 1.

The second case to be considered is when the laser beam is directed along the **B**-field direction and the laser is linearly polarized along the *x* axis. In this case, the "natural" quantization axis for the laser is along the polarization vector so that the target undergoes $\Delta m_J = 0$ transitions in this frame. However, this reference frame is orthogonal to the axis chosen when deriving Eqs. (22)–(24) and so cannot be adopted. It is therefore necessary to describe linearly polarized laser radiation as a superposition of σ^+ and σ^-. The amplitude components of the superposed polarization account for the direction of the incident linearly polarized radiation. For linear excitation, the magnitude of these components will be equal. For elliptically polarized radiation, the complex amplitudes of the two components will differ so as to create a net handedness and direction of the incident radiation [14].

A. Case 1: Circularly polarized laser excitation (B-field ∥ to laser direction)

In this configuration the quantization axis is chosen as in Fig. 1 and the laser promotes excitation from the $|0,0\rangle = |1\rangle$ *S*

state either to the $|1,-1\rangle = |2\rangle$ state using σ^- radiation or to the $|1,+1\rangle = |4\rangle$ state using σ^+ radiation. The $|1,0\rangle = |3\rangle$ state remains unpopulated in this frame of reference.

Consider excitation to the $|1,-1\rangle = |2\rangle$ state using σ^- radiation. In this case the only nonzero coupling coefficient is g_{21}^{-1} and the half Rabi frequency is Ω_{21}^{-1}. There is only one spontaneous emission route possible for this excitation process, which is relaxation back to the $|0,0\rangle = |1\rangle$ state. This configuration therefore represents a dynamic closed two-state process described by four coupled differential equations (see the Appendix for an example of the procedure to derive these equations)

$$\dot{\rho}_{11} = i\Omega_{21}^{-1}(\rho_{12} - \rho_{21}) + \Gamma_{21}\rho_{22},$$

$$\dot{\rho}_{22} = i\Omega_{21}^{-1}(\rho_{21} - \rho_{12}) - \Gamma_{21}\rho_{22},$$

$$\dot{\rho}_{12} = i\Omega_{21}^{-1}(\rho_{11} - \rho_{22}) - \left[\frac{\Gamma_{21}}{2} + i(\Delta_{L,31} + \omega_{B1})\right]\rho_{12},$$

$$\dot{\rho}_{21} = i\Omega_{21}^{-1}(\rho_{22} - \rho_{11}) - \left[\frac{\Gamma_{21}}{2} - i(\Delta_{L,31} + \omega_{B1})\right]\rho_{21}, \quad (27)$$

Note that the detuning can be incorporated into a single term:

$$\delta_{21} = \Delta_{L,31} + \omega_{B1}. \quad (28)$$

The equations of motion then exactly match those from any two-state closed system. In this case the detuning depends upon the magnetic **B** field through the Larmor frequency component ω_{B1}.

B. Case 2: Linearly polarized laser excitation (B ⊥ E)

For excitation using linearly polarized radiation where the polarization vector of the laser is orthogonal to the **B** field, the light vector must be decomposed into two orthogonal components whose reference axes are aligned with the **B** field. The result of this decomposition is that both the $|1,-1\rangle$ and $|1,+1\rangle$ states are *simultaneously* and *coherently* excited in the reference frame shown in Fig. 1. The equations of motion reflect this excitation by an appropriate choice of laser modes ($L = \pm 1$) and an appropriate choice of Rabi frequencies.

It can be shown that the relationship between the Rabi frequency in the reference frame of the laser polarization Ω_{eg}^{π} and that of the **B** field ($\Omega_{eg}^{\pm 1}$) is given by

$$\Omega_{eg}^{\pi_x} = \frac{1}{\sqrt{2}}(\Omega_{eg}^{-1} - \Omega_{eg}^{+1}), \quad (29)$$

where the convention of Corney [10] has been adopted for the circular basis states. Since excitation now involves three states ($|1\rangle, |2\rangle$, and $|4\rangle$), there will be nine coupled differential equations that must be solved simultaneously. The nonzero coupling coefficients are g_{21}^{-1} and g_{41}^{+1} and the half Rabi frequency is $\frac{1}{\sqrt{2}}(\Omega_{21}^{-1} - \Omega_{41}^{+1})$.

The full set of coupled differential equations are then given by (see the Appendix)

$$\dot{\rho}_{11} = i\Omega_{21}^{-1}(\rho_{12} - \rho_{21}) + i\Omega_{41}^{+1}(\rho_{14} - \rho_{41}) + \Gamma_{21}\rho_{22} + \Gamma_{41}\rho_{44},$$
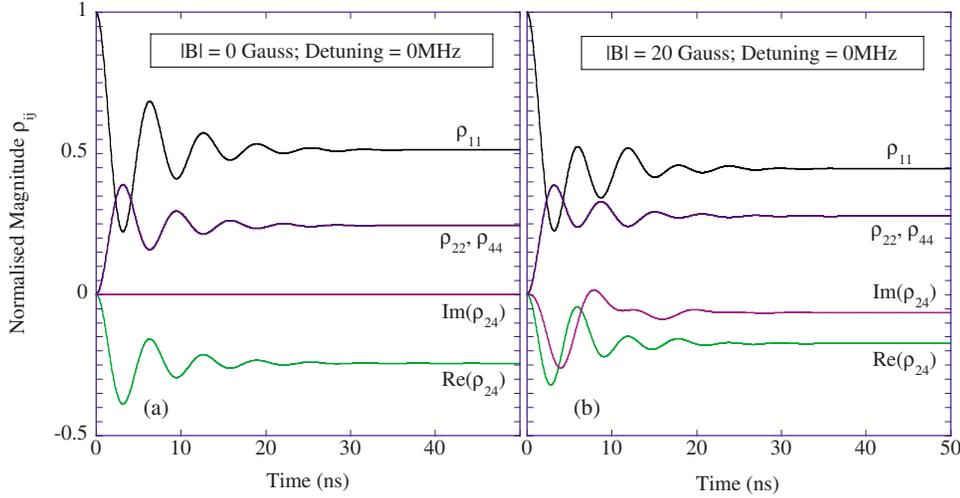
FIG. 2. (Color online) Calculation of the relative populations and atomic coherences of the upper $4\,^1P_1$ state of calcium excited using linearly polarized laser radiation with (a) zero magnetic field and (b) with a **B** field of 20 G. The laser detuning is set to $\Delta_{L,31}=0$ in this example, and so $\rho_{22}=\rho_{44}$. The population is normalized, so that $\rho_{11}+\rho_{22}+\rho_{44}=1$. For details, see text.

$$\dot{\rho}_{22} = +i\Omega_{21}^{-1}(\rho_{21}-\rho_{12})-\Gamma_{21}\rho_{22},$$

$$\dot{\rho}_{44} = +i\Omega_{41}^{+1}(\rho_{41}-\rho_{14})-\Gamma_{41}\rho_{44},$$

$$\dot{\rho}_{24} = +i\Omega_{41}^{+1}\rho_{21}-i\Omega_{21}^{-1}\rho_{14}-\left[\frac{1}{2}(\Gamma_{41}+\Gamma_{21})-2i\omega_{B1}\right]\rho_{24},$$

$$\dot{\rho}_{12} = +i\Omega_{21}^{-1}(\rho_{11}-\rho_{22})-i\Omega_{41}^{+1}\rho_{42}$$
$$-\left[\frac{\Gamma_{21}}{2}+i(\Delta_{L,21}+\omega_{B1})\right]\rho_{12},$$

$$\dot{\rho}_{14} = +i\Omega_{41}^{+1}(\rho_{11}-\rho_{44})-i\Omega_{21}^{-1}\rho_{24}$$
$$-\left[\frac{\Gamma_{41}}{2}+i(\Delta_{L,41}-\omega_{B1})\right]\rho_{14}$$

$$+ complex\ conjugates. \tag{30}$$

The equations no longer appear like those for a simple two-state system, and all participating populations $(\rho_{11},\rho_{22},\rho_{44})$, atomic coherences $(\rho_{24}=\rho_{42}^*)$, and optical coherences $(\rho_{12}=\rho_{21}^*; \rho_{14}=\rho_{41}^*)$ must be included. The atomic coherences $\rho_{24}=\rho_{42}^*$ are particularly interesting, as their equations contain an oscillatory term $(\pm 2i\omega_{B1})$ which results in precession of the charge cloud around the quantization axis. It is this term that leads to the familiar Hanle effect observed for electron or broadband photon excitation of an atomic state in a magnetic field.

It should also be noted that Eq. (30) reduces to the familiar two-state equations if the **B** field is set to zero ($\omega_{B1}=0$). The nine equations then reduce to the more familiar set of four for a two-state system involving states $|1\rangle$ and $|3\rangle$. This is accomplished using Eq. (27) and by applying a rotation operator to change the quantization axis from being parallel to the **B** field to being parallel to the polarization vector (**E** field) of the laser [13]:

$$\rho_{Jm,J'm'}^{B\ field}(t) = \sum_{\mu=-J}^{+J}\sum_{\mu'=-J'}^{+J'} D_{\mu m}^{J*}(\omega_E)\rho_{J\mu,J'\mu'}^{E\ field}(t)D_{\mu'm'}^{J'}(\omega_E). \tag{31}$$

The Euler angles for this rotation are given by

$$\omega_E = (\alpha_E,\beta_E,\gamma_E) = \left(0,+\frac{\pi}{2},0\right). \tag{32}$$

An important difference between the results from Eq. (30) and those observed in the Hanle effect is that the driving terms due to the laser field directly compete with the precessional motion of the atomic electrons due to the **B** field. Since the laser field is linearly polarized, Rabi oscillations between the ground and excited states attempt to maintain a P state aligned along the **E** field of the laser while the magnetic **B** field applies a torque to the atomic electrons causing them to precess around the **B** field axis. This competition results in oscillations of the charge cloud around the quantization axis which depend on the strength of the **B** field and the intensity of the laser radiation. Spontaneous emission damps out these oscillations so that, after a time typically greater than 10 times the lifetime of the upper state, the system reaches a steady state (to a good approximation as shown below) and the charge cloud aligns itself at a finite angle to the polarization direction of the laser.

A further consequence of the effects of the magnetic field is that there is a loss of coherence in the excited P state. The condition for loss of coherence is given by

$$\text{tr}\rho_{J=1}^2 - (\text{tr}\rho_{J=1})^2 = \delta_{tr}(t), \tag{33}$$

where $\delta_{tr}(t)\neq 0$.

Figure 2 shows dynamical results from Eq. (30) for excitation of calcium under the conditions where the magnetic field is (a) set to zero and (b) is 20 G and with a laser intensity of 25 mW/mm^2. The detuning is set to 0 MHz and the lifetime of the upper state is $\Gamma_{21}^{-1}=\Gamma_{41}^{-1}=4.6$ ns. Oscillations can be seen in the populations and atomic coherences due to only optical pumping in Fig. 2(a) and for both optical pumping and the magnetic field in Fig. 2(b). In particular, the
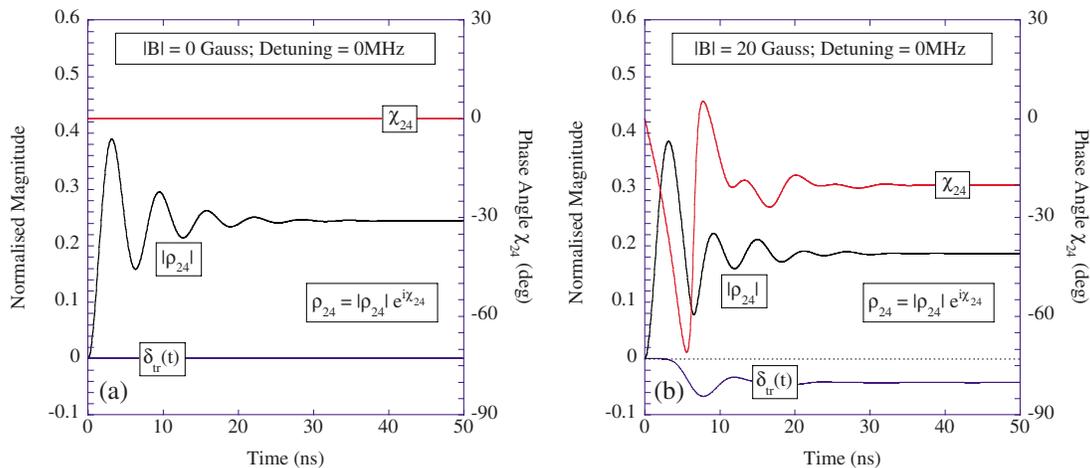
FIG. 3. (Color online) Calculation of the atomic coherence of the upper state ρ_{24} and the coherence parameter $\delta_{tr}(t)$ with (a) zero magnetic field and (b) with a **B** field of 20 G. The laser detuning $\Delta_{L,31}=0$ for a calcium target. The state is fully coherent with no **B** field, and the alignment angle is along the polarization vector. When a **B** field is applied, the P state oscillates around the **B** field, and there is a loss of coherence in the system.

atomic coherence $\rho_{24}=\mathrm{Re}(\rho_{24})+i\,\mathrm{Im}(\rho_{24})$ clearly shows the effect of the **B** field in the imaginary term. After $\sim$50 ns the system reaches a steady state, the oscillations are damped out, and the populations and coherences become stable.

Figure 3 shows the effect on $\rho_{24}(t)$ when rewritten as $\rho_{24}=|\rho_{24}|e^{i\chi_{24}}$. The phase angle χ_{24} remains constant at $\chi_{24}=0°$ when the **B** field is zero [Fig. 3(a)] and demonstrates a complex variation when the **B** field is applied [Fig. 3(b)]. The phase angle χ_{24} directly relates to the angle γ_P of the P-state charge cloud through the relationship $\chi_{24}=2\gamma_P$ (see below). Thus the variation of the charge cloud angle is directly related to this parameter.

Figure 3 further shows the effect of the **B** field on the coherence of the state as represented by $\delta_{tr}(t)$. When no **B** field is applied, $\delta_{tr}(t)=0$ and the state is fully coherent. By contrast, upon application of a **B** field, $\delta_{tr}(t)\neq 0$ and there is a loss of coherence. It can be shown that this is true in general when $\omega_{B1}\neq 0$.

The solutions to Eq. (30) as presented in Figs. 2 and 3 allow the angular "shape" of the charge cloud $W(\theta,\varphi)$ to be determined as a function of time, since we may write

$$W(\theta,\varphi) = \sum_{m_J,m_J'} \rho_{m_J m_J'} Y_{Jm_J}(\theta,\varphi) Y_{Jm_J'}^*(\theta,\varphi), \qquad (34)$$

where $Y_{Jm_J}(\theta,\varphi)$ is a spherical harmonic [15]. Figure 4 shows an example of this procedure at selected times between 0 ns (turn on of the laser field) and 50 ns (where steady-state conditions are reached). The results clearly show how the state oscillates and evolves around the quantization axis, reaching a steady-state angle which differs by $\sim$10° from that initially created by the laser beam (along the **E**-field direction). This is in accordance with the results in Fig. 3(b). A selection of movie files of the evolution of the state as a function of time over 50 ns for zero detuning, a laser intensity of 25 mW/mm², and **B** fields of 20 and 100 G can be seen in the supplementary material [23].

C. Steady-state conditions for S to P transitions

The steady-state solutions of the equations of motion, ρ_{ij}^{SS}, are derived by setting the time dependence in Eq. (25) to zero,

$$\underset{\sim}{A}\rho^{SS}=0, \qquad (35)$$

and the equations become simultaneous linear equations that can be solved using standard formalisms. For circular excitation [see Eq. (27)] the steady-state solutions are given by

$$\rho_{22}^{SS} = \frac{4\Omega_{21}^2}{8\Omega_{21}^2 + \Gamma_{21}^2 + 4(\Delta_{L,31} + \omega_{B1})^2},$$

$$\rho_{11}^{SS} = \frac{4\Omega_{21}^2 + \Gamma_{21}^2 + 4(\Delta_{L,31} + \omega_{B1})^2}{8\Omega_{21}^2 + \Gamma_{21}^2 + 4(\Delta_{L,31} + \omega_{B1})^2},$$
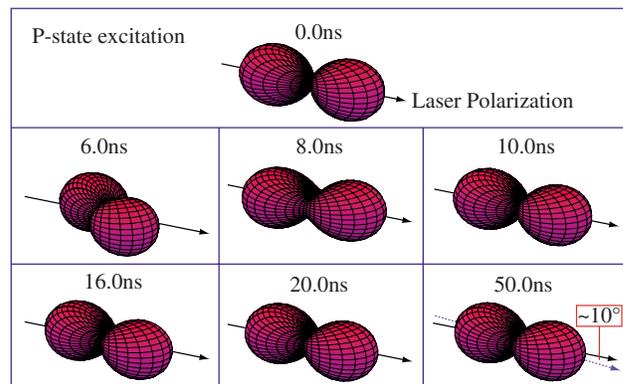

FIG. 4. (Color online) Examples of the angular shape of the P state for a **B** field of 20 G, derived from the results shown in Fig. 2. The state is seen to oscillate as a function of time, until it reaches a steady state $\sim$50 ns after initial excitation. The steady-state alignment angle is $\sim$10° from the direction of the exciting laser polarization vector.

$$\rho_{21}^{SS} = \frac{4\Omega_{21}(\Delta_{L,31} + \omega_{B1}) - 2i\Omega_{21}\Gamma_{21}}{8\Omega_{21}^2 + \Gamma_{21}^2 + 4(\Delta_{L,31} + \omega_{B1})^2}, \qquad (36)$$

where the population is normalized to unity: $\rho_{11}(t) + \rho_{22}(t) = 1$.

These equations are identical to those for a closed two-state system in the steady state, with additional detuning due to the **B** field. The force on the atom during laser cooling can then be calculated from the optical coherence ρ_{21}^{SS} in the usual way [1].

The steady-state solutions for π excitation are more involved, as Eq. (30) must now be solved setting the time dependence to zero. The solutions are given by

$$\rho_{11}^{SS} = \frac{A}{X}, \quad \rho_{22}^{SS} = \frac{B}{X}, \quad \rho_{44}^{SS} = \frac{C}{X}, \quad \rho_{24}^{SS} = \frac{D + iE}{X},$$

where

$$\begin{aligned}
A = {}& [4\omega_{B1}^2(3\Gamma^4 + 64\Delta_{L,31}^2\Omega^2 + 16\Gamma^2\Omega^2 + 16\Omega^4 \\
& + 16\Delta_{L,31}^4) + 16\omega_{B1}^4(3\Gamma^2 - 8\Delta_{L,31}^2) + 64\omega_{B1}^6 \\
& + 16\Omega^2(4\Gamma^2\Delta_{L,31}^2 + \Gamma^4) + 16\Omega^4(4\Delta_{L,31}^2 + 5\Gamma^2) \\
& + 128\Omega^6 \\
& + \Gamma^2(16\Delta_{L,31}^4 + 8\Delta_{L,31}^2\Gamma^2 + \Gamma^4)],
\end{aligned}$$

$$\begin{aligned}
B = {}& [4\Omega^2(-8\omega_{B1}\Gamma^2\Delta_{L,31} + 8\omega_{B1}^2(\Gamma^2 + 2\Delta_{L,31}^2 + 4\Omega^2) \\
& - 32\omega_{B1}^3\Delta_{L,31} + 16\omega_{B1}^4 + 8\Omega^2\Gamma^2 + 16\Omega^4 \\
& + 4\Gamma^2\Delta_{L,31}^2 + \Gamma^4)],
\end{aligned}$$

$$\begin{aligned}
C = {}& [4\Omega^2(8\omega_{B1}\Gamma^2\Delta_{L,31} + 8\omega_{B1}^2(\Gamma^2 + 2\Delta_{L,31}^2 + 4\Omega^2) \\
& + 32\omega_{B1}^3\Delta_{L,31} + 16\omega_{B1}^4 + 8\Omega^2\Gamma^2 + 16\Omega^4 \\
& + 4\Gamma^2\Delta_{L,31}^2 + \Gamma^4)],
\end{aligned}$$

$$\begin{aligned}
D = {}& [-4\Omega^2(16\omega_{B1}^2\Delta_{L,31}^2 - 16\omega_{B1}^4 + 8\Omega^2\Gamma^2 \\
& + 16\Omega^4 + 4\Gamma^2\Delta_{L,31}^2 + \Gamma^4)],
\end{aligned}$$

$$E = [-16\omega_{B1}\Omega^2\Gamma(\Gamma^2 + 4\Omega^2 + 4\omega_{B1}^2)],$$

$$\begin{aligned}
X = {}& [4\omega_{B1}^2(3\Gamma^4 + 96\Delta_{L,31}^2\Omega^2 + 32\Gamma^2\Omega^2 + 80\Omega^4 + 16\Delta_{L,31}^4) \\
& + 16\omega_{B1}^4(3\Gamma^2 - 8\Delta_{L,31}^2 + 8\Omega^2) + 64\omega_{B1}^6 \\
& + 24\Omega^2(4\Gamma^2\Delta_{L,31}^2 + \Gamma^4) + 16\Omega^4(4\Delta_{L,31}^2 + 9\Gamma^2) \\
& + 256\Omega^6 + \Gamma^2(16\Delta_{L,31}^4 + 8\Delta_{L,31}^2\Gamma^2 + \Gamma^4)], \qquad (37)
\end{aligned}$$

where $\Omega = \frac{\Omega_{31}^{\pi x}}{\sqrt{2}}$, $\Gamma = \Gamma_{21} = \Gamma_{41}$, and the total population has again been set to unity: $\rho_{11}(t) + \rho_{22}(t) + \rho_{44}(t) = 1$. These equations reduce to the equivalent two-state solutions if the **B** field is set to zero (ie $\omega_{B1} = 0$) as required.

The advantage of using the steady-state solutions given in Eqs. (36) and (37) is that these yield *analytic* solutions to the populations and coherences of the system under study. Since in an experiment the interaction with the laser may occur over a time period far longer than it takes the system to reach equilibrium, these solutions often prove to be an accurate representation. As an example, for calcium effusing from an
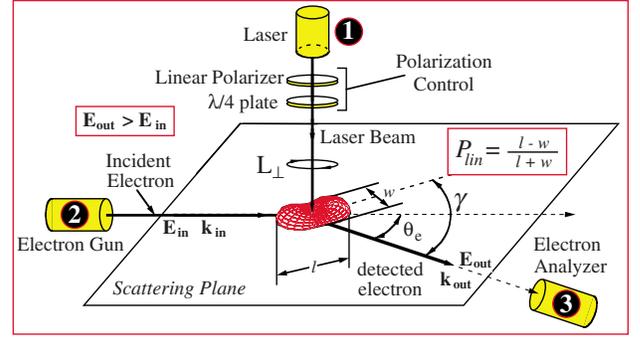

FIG. 5. (Color online) The superelastic scattering geometry, showing the scattering plane, the direction of the laser beam, and the natural frame parameters that are used to define the state.

atomic beam oven at 1000 K, the average velocity of the atoms is $\sim$720 m/s. If the atoms enter a laser beam of diameter 1 mm, the interaction time is $\sim$1400 ns—far longer than the 50 ns required to reach dynamic equilibrium. In this case, Eqs. (36) and (37) give an accurate description of the atomic system under the influence of the laser and magnetic fields.

Finally note that the coherence parameter δ_{tr} and angle of the P state γ_P can also be directly derived in the steady state. In this case,

$$\delta_{tr}^{SS} = \rho_{24}^{SS}\rho_{42}^{SS} - \rho_{22}^{SS}\rho_{44}^{SS} = \frac{D^2 + E^2 - BC}{X^2}, \quad \tan 2\gamma_P^{SS} = \frac{E}{D}. \qquad (38)$$

From these expressions it can be shown that $\delta_{tr}^{SS} = 0$; $\gamma_P^{SS} = 0$ when $\omega_{B1} = 0$ (i.e., when $|\mathbf{B}| = 0$). Further, it can be shown for high **B** fields (within the approximations of the model) that

$$\gamma_P^{SS} \underset{\omega_{B1} \to \infty}{\longrightarrow} \pm\frac{\pi}{2}. \qquad (39)$$

The P state therefore tends to align orthogonal to the laser polarization vector when the **B** field is high.

IV. EXAMPLE: APPLICATION TO SUPERELASTIC SCATTERING IN A B FIELD

Superelastic scattering of electrons from laser prepared atoms is a powerful technique which can measure excitation cross sections for inelastic electron scattering [4,16–22]. This is possible since superelastic scattering can be considered as the time inverse of coincidence methods which time-correlate the electron that excites an atom with the photon emitted during relaxation. Figure 5 shows the principle of the superelastic scattering method. A laser beam of well-defined polarization and energy (1) excites the atom and an electron of energy E_{inc} and momentum $\mathbf{k}_{inc}$ (2) then scatters superelastically from the excited P-state target. The electron scatters at an angle θ_e with momentum $\mathbf{k}_{out}$, thereby defining a scattering plane. This electron is detected by an analyzer (3), and the rate of scattered electrons is determined as a function of the laser polarization and scattering angle.

From these results, the excitation cross section is determined. The superelastic signal as a function of the laser polarization $S^{polzn}(\theta_e)$ is given by [16]

$$S^{polzn}(\theta_e) = \sum_{m_J, m_J'} \rho_{m_J, m_J'}^{laser} \rho_{m_J, m_J'}^{deexc}(\theta_e) = \sum_{m_J, m_J'} \rho_{m_J, m_J'}^{laser} \rho_{m_J', m_J}^{exc}(\theta_e),$$

$$(40)$$

where $\rho_{m_J, m_J'}^{laser}$ is the density matrix for the upper state created by the laser in the **B** field, $\rho_{m_J, m_J'}^{deexc}(\theta_e)$ is the density matrix for electron deexcitation of this state, and $\rho_{m_J, m_J'}^{exc}(\theta_e)$ is the density matrix for the equivalent excitation process.

By choosing a quantization z axis given by the direction of the **B** field and by taking measurements where the scattering plane is orthogonal to the z axis, the excitation density matrix can be defined in the natural frame. In this case, assuming no electron spin flip occurs, we may write

$$\rho_{m_J, m_J'}^{exc}(\theta_e) = \frac{1}{2} \begin{pmatrix} 1 + L_\perp(\theta_e) & 0 & -P_{lin}(\theta_e)e^{+2i\gamma_e(\theta_e)} \\ 0 & 0 & 0 \\ -P_{lin}(\theta_e)e^{-2i\gamma_e(\theta_e)} & 0 & 1 - L_\perp(\theta_e) \end{pmatrix},$$

$$(41)$$

where $L_\perp(\theta_e)$ defines the angular momentum transferred to the atom orthogonal to the scattering plane during the collision, $P_{lin}(\theta_e)$ defines the "length" to "width" ratio of the charge cloud, and $\gamma_e(\theta_e)$ defines the angle of the charge cloud with respect to the scattered electron, as in Fig. 5.

A. Case 1: Circularly polarized laser excitation

As an example of the use of Eq. (40), consider circular excitation prior to the electron collision. In this case,

$$(\rho_{m_J, m_J'}^{laser})^{\sigma^+} = \begin{pmatrix} \rho_{22} & 0 & 0 \\ 0 & 0 & 0 \\ 0 & 0 & 0 \end{pmatrix}, \quad (\rho_{m_J, m_J'}^{laser})^{\sigma^-} = \begin{pmatrix} 0 & 0 & 0 \\ 0 & 0 & 0 \\ 0 & 0 & \rho_{44} \end{pmatrix},$$

$$\therefore S^{\sigma^+}(\theta_e) = \sum_{m_J, m_J'} \rho_{m_J, m_J'}^{laser} \rho_{m_J', m_J}^{exc}(\theta_e) = \frac{1}{2}\rho_{22}(1 + L_\perp),$$

$$\therefore S^{\sigma^-}(\theta_e) = \sum_{m_J, m_J'} \rho_{m_J, m_J'}^{laser} \rho_{m_J', m_J}^{exc}(\theta_e) = \frac{1}{2}\rho_{44}(1 - L_\perp). \quad (42)$$

The superelastic scattering signal determines the pseudo-Stokes parameter $P_3^S(\theta_e)$ [16], and so

$$P_3^S(\theta_e) = \frac{S^{\sigma^+}(\theta_e) - S^{\sigma^-}(\theta_e)}{S^{\sigma^+}(\theta_e) + S^{\sigma^-}(\theta_e)} = \frac{(\rho_{22} - \rho_{44}) + L_\perp(\rho_{44} + \rho_{22})}{(\rho_{44} + \rho_{22}) + L_\perp(\rho_{22} - \rho_{44})}.$$

$$(43)$$

Under steady-state conditions the relative populations are given by

$$\rho_{22}^{SS} = \frac{4\Omega_{21}^2}{8\Omega_{21}^2 + \Gamma_{21}^2 + 4(\Delta_{L,31} + \omega_{B1})^2},$$

$$\rho_{44}^{SS} = \frac{4\Omega_{21}^2}{8\Omega_{21}^2 + \Gamma_{21}^2 + 4(\Delta_{L,31} - \omega_{B1})^2}. \quad (44)$$

To determine $L_\perp$ directly from experiment, it is therefore necessary to tune the laser to resonance with states $|2\rangle$ and $|4\rangle$ prior to measuring the scattering rates. In this case,

$$\rho_{22}^{SS} \underset{(\Delta + \omega_{B1})=0}{\rightarrow} \frac{4\Omega_{21}^2}{8\Omega_{21}^2 + \Gamma_{21}^2}, \quad \rho_{44}^{SS} \underset{(\Delta - \omega_{B1})=0}{\rightarrow} \frac{4\Omega_{21}^2}{8\Omega_{21}^2 + \Gamma_{21}^2} = \rho_{22}^{SS},$$

$$(45)$$

and so

$$L_\perp = P_3^S(\theta_e). \quad (46)$$

This is equivalent to that derived for a conventional superelastic experiment which does not use a **B** field. The difference between experiments arises since upon application of a **B** field (as from a MAC device), the laser frequency must be adjusted to be on resonance with each selected state as the laser polarization switches from σ^+ to σ^- [4].

B. Case 2: Linearly polarized laser excitation

Calculation of the superelastic signal for linear laser excitation in the **B** field is more complex than for circular excitation. The density matrix in the laser frame of reference is defined with the x axis aligned along the laser polarization vector, which is assumed to make an angle ε to the x axis in the natural frame. It is therefore necessary to align both frames using rotation operators prior to application of Eq. (41) to determine the superelastic scattering signal rates. Steady-state conditions are assumed in the following derivation.

Alignment of the laser frame to the natural frame requires a rotation through Euler angles $(\alpha^E, \beta^E, \gamma^E) = (\varepsilon, 0, 0)$—i.e., rotation around the z axis through an angle ε. The density matrix for laser excitation in the natural frame is then given by

$$\rho_{ij}^{L(nat)} = \frac{1}{X} \begin{pmatrix} C & 0 & Me^{-2i(\gamma_P^{SS}+\varepsilon)} \\ 0 & 0 & 0 \\ Me^{+2i(\gamma_P^{SS}+\varepsilon)} & 0 & B \end{pmatrix},$$

$$M = \sqrt{D^2 + E^2}, \quad \tan 2\gamma_P^{SS} = \frac{E}{D}. \quad (47)$$

Application of Eq. (40) allows the superelastic signal to be derived for π-polarized light. In this case,

$$S^\varepsilon(\theta_e) = \frac{(B + C) + L_\perp(\theta_e)(B - C)}{2X}$$

$$- \frac{\sqrt{D^2 + E^2}}{X} P_{lin}(\theta_e)\cos 2[\gamma(\theta_e) + \gamma_P^{SS} + \varepsilon]. \quad (48)$$

Note that the superelastic signal contains terms in $L_\perp(\theta_e)$ as well as in $P_{lin}(\theta_e)$ and $\gamma(\theta_e)$. This is expected, as the detuning $\Delta_{L,31}$ will favor excitation of the state closest to resonance with the laser, producing both alignment and orienta-

tion of the target. Equation (48) simplifies when $\Delta_{L,31}=0$ (i.e., the laser is resonant with state $|3\rangle$), since under these conditions $B=C$. In this case,

$$S^\varepsilon(\theta_e) \underset{\Delta_{L,31}=0}{\to} \frac{B}{X} - \frac{\sqrt{D^2+E^2}}{X}P_{lin}(\theta_e)\cos 2[\gamma(\theta_e) + \gamma_P^{SS} + \varepsilon].$$

(49)

Determination of the alignment angle $\gamma(\theta_e)$ can therefore be achieved by varying the laser polarization angle ε and fitting Eq. (49) to the data. The resulting phase shift then directly relates to $\gamma(\theta_e)+\gamma_P^{SS}$, where γ_P^{SS} is a constant set by the laser and **B**-field parameters. γ_P^{SS} can be determined by comparing $S^\varepsilon(\theta_e)$ with and without the **B** field, thus establishing the constant offset γ_P^{SS} (which is independent of the scattering angle θ_e).

$P_{lin}(\theta_e)$ can be measured either by fitting experimental data to Eq. (49) or by determining the pseudo-Stokes parameters $P_{1,2}^S(\theta_e)$ [16]. In either case, the fitted parameter is scaled by a factor that depends on the laser and **B** fields. When fitted to Eq. (49), $P_{lin}(\theta_e)$ can be determined from the maximum and minimum of the function:

$$S^\varepsilon_{\max}(\theta_e) = \frac{B}{X} + \frac{\sqrt{D^2+E^2}}{X}P_{lin}(\theta_e),$$

$$S^\varepsilon_{\min}(\theta_e) = \frac{B}{X} - \frac{\sqrt{D^2+E^2}}{X}P_{lin}(\theta_e),$$

$$\Rightarrow P_{lin}(\theta_e) = \kappa \frac{S^\varepsilon_{\max}(\theta_e) - S^\varepsilon_{\min}(\theta_e)}{S^\varepsilon_{\max}(\theta_e) + S^\varepsilon_{\min}(\theta_e)},$$

where

$$\kappa = \frac{B}{\sqrt{D^2+E^2}}.$$

(50)

Note that when the **B** field is zero, $D=-B$, $E=0$, and so $\kappa=1$. Hence the value of κ can be determined by taking experimental data with and without the **B** field operating so as to determine $S^\varepsilon_{\max}(\theta_e)$, $S^\varepsilon_{\min}(\theta_e)$, and $P_{lin}(\theta_e)$ in both cases. κ is then given by the ratio of these measurements. Since κ does not depend on the scattering angle θ_e, the value of κ can be used throughout all measurements of $P_{lin}(\theta_e)$ when the **B** field is present (e.g., in regions where it is not possible to measure the superelastic signal using a conventional spectrometer). Experiments of this type have now been carried out and results are discussed in Refs. [4,22].

V. CONCLUSIONS

In this paper a QED model for the interaction of laser radiation with a target immersed in a magnetic field has been derived where the **B** field is assumed to produce a small perturbation to the energy levels. The model yields a set of three general equations of motion that relate to the populations of the states and their relative phases (coherences). The quantization axis was chosen along the **B**-field direction and

the equations derived with respect to this axis.

Examples of the use of these equations applied to actual experimental geometries were then given, specifically when the laser beam was circularly and linearly polarized. The equations were solved under these conditions for an S-state to P-state transition, the dynamics being studied using calcium as an example. For circular excitation, it was shown that the model is identical to a two-state system with appropriate choice of detuning. For linear excitation, the model shows that the state oscillates around the quantization axis before coming to rest at a set angle to the polarization vector of the laser beam. The coherence of the state was also seen to reduce with application of the magnetic field.

The steady-state equations were then derived and solutions presented. These were used in the example of superelastic electron scattering from laser prepared calcium where it was shown that the natural frame parameters can be derived from experiment. The combination of laser and magnetic fields was found to change the alignment angle γ of the state by a constant offset angle γ_P^{SS}, whereas the alignment parameter P_{lin} was found to scale by a constant factor κ. Both γ_P^{SS} and κ can be determined directly from experiment by comparing the results with and without the **B** field at a given scattering angle θ_e. The orientation parameter $L_\perp$ was seen to be directly measurable from the data providing the laser was tuned to resonance for each polarization $\sigma^\pm$ state of the laser.

The theory presented here should find applicability in a wide variety of experiments. Since the dynamics of the interaction can be calculated accurately, this opens up the possibility of carrying out new types of experiments where these dynamics are exploited. Further, since the model is not confined to the simple two-state system widely adopted by many researchers, it will allow researchers to understand and optimize their experiments to a higher degree. Derivation of the equations of motion is straightforward, and solutions can be found using basic computer systems as located in most research laboratories. The model is presently being used for both superelastic and atom cooling experiments in Manchester, and it is hoped that other researchers will also benefit from the results presented here.

APPENDIX: EXAMPLE OF THE DERIVATION OF THE EQUATIONS OF MOTION

Circular excitation case

Consider excitation to the $|1,-1\rangle=|2\rangle$ state using σ^- radiation. For the lower state, Eq. (22) reduces to

$$\dot{\rho}_{gg''} = -i(\omega_g - \omega_{g''} + \omega_{BJ_g} m_g - \omega_{BJ_{g''}} m_{g''})\rho_{gg''} + i\sum_{L,e}\Omega^L_{eg''}\rho_{ge} - i\sum_{L,e}\Omega^L_{eg}\rho_{eg''}$$

$$+ \sum_{\lambda',e',e''} g^{\lambda'}_{e'g''} g^{\lambda'*}_{e''g} \pi\delta(\Delta_{e''g} - \omega_{\lambda'})\rho_{e''e'} + \sum_{\lambda',e',e''} g^{\lambda'*}_{e'g} g^{\lambda'}_{e''g''} \pi\delta(\omega_{\lambda'} - \Delta_{e''g''})\rho_{e'e''} \Rightarrow \dot{\rho}_{11}$$

$$= -i(\omega_1 - \omega_1 + \omega_{BJ_1} \cdot 0 - \omega_{BJ_1} \cdot 0)\rho_{11} + i\sum_{L,e}\Omega^L_{e1}\rho_{1e} - i\sum_{L,e}\Omega^L_{e1}\rho_{e1}$$

$$+ \sum_{\lambda',e',e''} g^{\lambda'}_{e'1} g^{\lambda'*}_{e''1} \pi\delta(\Delta_{e''1} - \omega_{\lambda'})\rho_{e''e'} + \sum_{\lambda',e',e''} g^{\lambda'*}_{e'1} g^{\lambda'}_{e''1} \pi\delta(\omega_{\lambda'} - \Delta_{e''1})\rho_{e'e''}$$

$$= 0 + i\Omega^{-1}_{21}\rho_{12} - i\Omega^{-1}_{21}\rho_{21} + g^{-1}_{21} g^{-1*}_{21} \pi\delta(\Delta_{21} - \omega_{-1})\rho_{22} + g^{-1*}_{21} g^{-1}_{21} \pi\delta(\omega_{-1} - \Delta_{21})\rho_{22}$$

$$= i\Omega^{-1}_{21}(\rho_{12} - \rho_{21}) + 2|g^{-1}_{21}|^2 \pi\delta(\Delta_{21} - \omega_{-1})\rho_{22} \Rightarrow \dot{\rho}_{11} = i\Omega^{-1}_{21}(\rho_{12} - \rho_{21}) + \Gamma_{21}\rho_{22}. \tag{A1}$$

The excited-state population ρ_{22} and optical coherences $\rho_{21} = \rho^*_{12}$ can be derived in a similar way. This leads to the set of four coupled differential equations which are given in Eq. (27).

Linear excitation case

An example is given for the lower state under linear excitation to again illustrate the process. From Eq. (22),

$$\dot{\rho}_{gg''} = -i(\omega_g - \omega_{g''} + \omega_{BJ_g} m_g - \omega_{BJ_{g''}} m_{g''})\rho_{gg''} + i\sum_{L,e}\Omega^L_{eg''}\rho_{ge} - i\sum_{L,e}\Omega^L_{eg}\rho_{eg''}$$

$$+ \sum_{\lambda',e',e''} g^{\lambda'}_{e'g''} g^{\lambda'*}_{e''g} \pi\delta(\Delta_{e''g} - \omega_{\lambda'})\rho_{e''e'} + \sum_{\lambda',e',e''} g^{\lambda'*}_{e'g} g^{\lambda'}_{e''g''} \pi\delta(\omega_{\lambda'} - \Delta_{e''g''})\rho_{e'e''} \therefore \dot{\rho}_{11}$$

$$= -i(\omega_1 - \omega_1 + \omega_{BJ_1} \cdot 0 - \omega_{BJ_1} \cdot 0)\rho_{11} + i\sum_{L,e}\Omega^L_{e1}\rho_{1e} - i\sum_{L,e}\Omega^L_{e1}\rho_{e1}$$

$$+ \sum_{\lambda',e',e''} g^{\lambda'}_{e'1} g^{\lambda'*}_{e''1} \pi\delta(\Delta_{e''1} - \omega_{\lambda'})\rho_{e''e'} + \sum_{\lambda',e',e''} g^{\lambda'*}_{e'1} g^{\lambda'}_{e''1} \pi\delta(\omega_{\lambda'} - \Delta_{e''1})\rho_{e'e''}$$

$$= 0 + i\Omega^{-1}_{21}\rho_{12} + i\Omega^{+1}_{41}\rho_{14} - i\Omega^{-1}_{21}\rho_{21} - i\Omega^{+1}_{41}\rho_{41} + g^{-1}_{21} g^{-1*}_{21} \pi\delta(\Delta_{21} - \omega_{-1})\rho_{22} + g^{+1}_{41} g^{+1*}_{41} \pi\delta(\Delta_{41} - \omega_{+1})\rho_{44}$$

$$+ g^{-1*}_{21} g^{-1}_{21} \pi\delta(\omega_{-1} - \Delta_{21})\rho_{22} + g^{+1*}_{41} g^{+1}_{41} \pi\delta(\omega_{+1} - \Delta_{41})\rho_{44}$$

$$= i\Omega^{-1}_{21}(\rho_{12} - \rho_{21}) + i\Omega^{+1}_{41}(\rho_{14} - \rho_{41}) + 2|g^{-1}_{21}|^2 \pi\delta(\Delta_{21} - \omega_{-1})\rho_{22} + 2|g^{+1}_{41}|^2 \pi\delta(\Delta_{41} - \omega_{+1})\rho_{44}$$

$$\Rightarrow \dot{\rho}_{11} = i\Omega^{-1}_{21}(\rho_{12} - \rho_{21}) + i\Omega^{+1}_{41}(\rho_{14} - \rho_{41}) + \Gamma_{21}\rho_{22} + \Gamma_{41}\rho_{44}. \tag{A2}$$

The full set of nine coupled equations can be derived in a similar way, as given by Eq. (30).

[1] H. J. Metcalf and P. van der Straten, *Laser Cooling and Trapping* (Springer, New York, 1999), and references therein.

[2] F. H. Read and J. M. Channing, Rev. Sci. Instrum. **67**, 2372 (1996).

[3] B. Mielewska, I. Linert, G. C. King, and M. Zubek, Phys. Rev. A **69**, 062716 (2004).

[4] M. Hussey, A. J. Murray, W. R. MacGillivray, and G. C. King, Phys. Rev. Lett. **99**, 133202 (2007).

[5] G. C. King, in *Electron Scattering*, edited by C. T. Whelan and N. J. Mason (Springer, Berlin, 2006), p. 111, and references therein.

[6] N. J. Bowring, F. H. Read, and A. J. Murray, J. de Physique **9**, Pr6-45-49 (1999).

[7] M. A. Stevenson and B. Lohmann, Phys. Rev. A **73**, 020701(R) (2006).

[8] R. Loudon, *The Quantum Theory of Light* (Oxford University Press, Oxford, 1995).

[9] P. M. Farrell, W. R. MacGillivray, and M. C. Standage, Phys. Rev. A **37**, 4240 (1988).

[10] A. Corney, *Atomic and Laser Spectroscopy* (Oxford University Press, Oxford, 2006).

[11] J. R. Ackerhalt and J. H. Eberly, Phys. Rev. D **10**, 3350 (1974).

[12] A. J. Murray, W. R. MacGillivray, and M. C. Standage, J. Phys. B **23**, 3373 (1990).

[13] W. R. MacGillivray and M. C. Standage, Phys. Rep. **168**, 1 (1988).

[14] B. T. H. Varcoe, R. T. Sang, W. R. MacGillivray, M. C. Standage, and P. M. Farrell, J. Mod. Opt. **46**, 787 (1999).

[15] A. T. Masters, A. J. Murray, R. Pascual, and M. C. Standage, Phys. Rev. A **53**, 3884 (1996).

[16] I. V. Hertel and W. Stoll, Adv. At. Mol. Phys. **13**, 113 (1977).

[17] A. J. Murray and D. Cvejanovic, J. Phys. B **36**, 4889 (2003).

[18] B. V. Hall, M. Shurgalin, A. J. Murray, W. R. MacGillivray, and M. C. Standage, Aust. J. Phys. **52**, 515 (1999).

[19] P. M. Farrell, W. R. MacGillivray, and M. C. Standage, Phys. Rev. A **44**, 1828 (1991).

[20] P. W. Zetner, P. V. Johnson, Y. Li, G. Csanak, R. E. H. Clark, and J. Abdallah, Jr., J. Phys. B **34**, 1619 (2001).

[21] M. R. Law and P. J. O. Teubner, J. Phys. B **28**, 2257 (1995).

[22] M. J. Hussey, A. J. Murray, W. R. MacGillivray, and G. C. King (unpublished).

[23] See EPAPS Document No. E-PLRAAN-77-089801 for a selection of movie files of the evolution of the steady state as a function of time over 50 ns for zero detuning, a laser intensity of 25 mW/mm^2, and **B** fields of 20 and 100 G. For more information on EPAPS, see http://www.aip.org/pubservs/epaps.html.